Segmentation of multispectral images in optical metallography

E. Pirard*, V. Bertholet**

* MICA, Université de Liège, Belgique
** Département Mathématique, Faculté Universitaire ND de la Paix, Namur, Belgique

The use of adequate multispectral image acquisition and segmentation procedures is essential for automatic phase identification in metallography. Spatial and supervised spectral classification methods are compared on a set of five different optical ore micrographs. Nearest neighbour classification complemented by a geodesic propagation filter appears to give the best results. This method is often able to rival with EDX mapping where cost and speed are essential parameters.

■ INTRODUCTION

Ore microscopy is an essential tool for performing quality control of process operations in the mineral industry. Mineralogical species identification, grain size distributions and particle liberation statistics are among the most important questions to be answered from microscopical observations (1). Optical image analysis has the advantage of simplicity and cost, but its use in mineralogical studies remains confidential and more research has been dedicated to the development of automatic or semi-automatic quantitative measurements based on back scattered electron (BSE) images or energy dispersive X-ray (EDX) images (2).

Considering that a trained human operator is able to distinguish the main mineral species under simple polarized reflected light microscopy, it is worth trying to develop a colour image analysis system for ore microscopy at least as a preliminary step to more detailed investigation under the scanning electron microscope (SEM).

Quantitative spectral analysis has a long tradition in mineralogy (3, 4) and a systematic compilation of reflectance data has already been published together with detailed microprobe analyses (5). From these data, it is obvious that minerals do not display a very wide variety of colours in reflected light. Their reflectance spectra are smooth curves with no characteristic peaks in the visible region (*fig. 1*). Nevertheless, colour differences between major ore minerals are often strong enough to be used for pixel classification in mineralogical images if a careful image acquisition procedure is followed. The acquisition methodology involving correction for heterogeneous response of the whole system (CCD, microscope, light) as well as checking the linearity and thermal stability of the camera response has been presented elsewhere (6). It must be clear that without ensuring a proper mapping of the reflectance properties to the grey level scale, there is little hope to get satisfactory results from optical image analysis. It is the aim of this paper to apply some classification techniques currently used in remote sensing on metallographical images and to compare their relative performance.

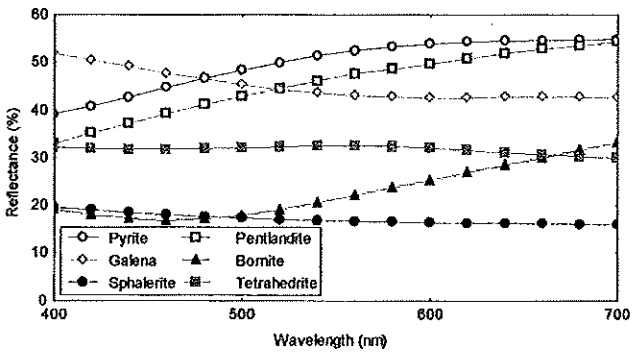

Figure 1. – Reflectance spectra in the visible range for some major sulphide minerals. Quantitative data at 20 nm interval are taken from (5).

Figure 1. – Spectre de réflectance spéculaire dans le domaine visible de quelques minéraux sulfurés importants. Les mesures quantitatives prises tous les 20 nm sont extraites de (5).

Manuscrit reçu le 4 janvier 1999, bon à publier le 22 mai 1999.

Segmentation des images multispectrales en métallographie optique

E. Pirard*, V. Bertholet**

* MICA, Université de Liège, Belgique
** Département Mathématique, Faculté Universitaire ND de la Paix, Namur, Belgique

L'analyse d'images en métallographie optique prend tout son intérêt lorsqu'elle permet de déboucher sur des méthodes entièrement automatisées. Pour aboutir à cela, il convient d'être particulièrement attentif aux procédures d'acquisition des images multispectrales et aux outils statistiques de classification des pixels.

Toutes les images multispectrales doivent faire l'objet de corrections qui prennent en compte les inégalités de réponse du système (CCD, optique, éclairage). Ces corrections sont tant spatiales (vignettage de l'optique) que temporelles (bruit thermique du CCD). L'utilisation de standards de réflectance est essentielle pour permettre une calibration de l'échelle des réflectances et pour faire une balance *des blancs qui a pour objet de corriger les variations de sensibilité du capteur en fonction de la longueur d'onde.*

Cet article part d'un ensemble d'images prises sur des minerais d'origine très diverses pour faire une analyse comparative des principales méthodes d'analyse discriminante supervisée disponibles. Directement issues de la télédétection, ces méthodes sont encore peu utilisées en microscopie. Après une phase d'apprentissage durant laquelle l'opérateur désigne un ensemble de pixels qu'il juge représentatifs de chaque minéral présent dans l'image, l'algorithme de classification supervisée juge de la proximité *des pixels non-classés avec les classes ainsi définies par l'opéateur. La* proximité *peut s'évaluer soit en regard d'un modèle statistique (multigaussien), soit en regard d'une mesure quelconque dans l'espace spectral (distance euclidienne, volume de l'enveloppe convexe des pixels de même classe). Il ressort des résultats comparatifs sur quatre méthodes, que celle dite « du plus proche voisin » offre un bon compromis entre complexité algorithmique et pertinence de la classification. Pour être complète, une segmentation ne peut s'effectuer sur les seuls critères spectraux ; c'est pourquoi une analyse spatiale du contexte local de chaque pixel permet de filtrer les images et d'améliorer encore les résultats. Nous introduisons dans cet article une méthode originale basée sur des dilatations et des propagations géodésiques. Quoique très simple dans son principe, ce filtre s'avère performant et très intuitif pour les images rencontrées en métallographie. En conclusion, il est permis de penser que l'analyse d'images optiques peut rivaliser dans bon nombre de cas avec des méthodes beaucoup plus coûteuses et beaucoup plus lourdes telles que l'imagerie en électrons rétrodiffusés ou la cartographie élémentaire en énergie dispersive des rayons X (EDX).*

*La segmentation entre pyrite, pentlandite et chalcopyrite, trois minéraux majeurs dans les minerais de nickel, constitue une bonne illustration de la méthode. L'analyse d'images prise sans précautions, que ce soit en noir et blanc ou en couleur, échoue généralement dans la différenciation entre la pyrite et la pentlandite. Les deux minéraux sont fort semblables et même difficiles à différencier pour un microscopiste peu expérimenté. En imagerie d'électrons rétrodiffusés, c'est le couple chalcopyrite/pentlandite qui est indifférenciable car les deux phases présentent un nombre atomique moyen de 23,7. Enfin en EDX, il conviendrait de réaliser une triple image Ni, Fe, Cu, pour diffeencier avec certitude les trois minéraux. Considérant une résolution classique en optique de 512*512 pixels, ceci peut prendre quelques heures d'analyse. L'utilisation d'une imagerie RGB proprement calibrée permet un taux de reconnaissance des phases satisfaisant pour les besoins d'une analyse modale du minerai.*

■ IMAGING AND SEGMENTATION METHODS

RGB imaging of ore micrographs

Instead of using truly multispectral images with no overlapping of the spectral bands, the images used in this paper are RGB images in the sense that they refer to the red (R), green (G) and blue (B) filters defined by the C.I.E. for colorimetric purposes (*fig. 2*). The spectral overlapping due to the rather large bandwidth (± 40 nm) of the R,G and B filters implies a redundancy of information between the three images. A better imaging approach would consist in taking interference filters with a narrower bandwidth (± 2 nm) and optimizing the wavelength selection with respect to the phases to be discriminated in the ore.

A set of five polished sections, representing major sulphide parageneses, has been selected for testing the classification methods (*table I*). The number of major phases within each ore is rather limited (4 to 6) and one could expect from

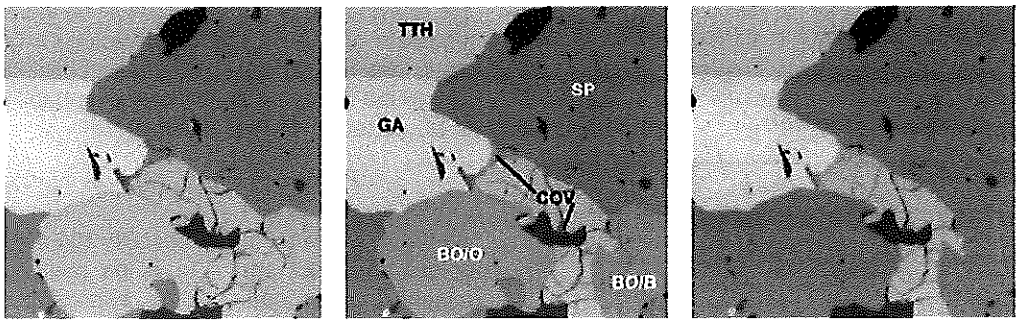

Figure 2. – Red, green and blue images from the Kipushi copper ore with tetraedrite (Tth), galena (Ga), sphalerite (Sp), orange bornite (Bo/O), brown bornite (Bo/B) and covellite (Cov).

Figure 2. – Images rouge, verte et bleue du minerai de cuivre de Kipushi avec de la tétrahédrite (Tth), de la galène (Ga), de la sphalérite (Sp), de la bornite orange (Bo/O), de la bornite brune (Bo/B) et de la covelline (Cov).

TABLE I. – Polished sections used for colour image segmentation experiments.

TABLEAU I. – Liste des sections polies utilisées pour les essais de segmentation couleur.

Code	Locality	Minerals
EP833	Panasqueira (Portugal)	Arsenopyrite, chalcopyrite, pyrrhotite, pyrite, sphalerite
M12	Sudbury (Canada)	Chalcopyrite, pentlandite, pyrrhotite, pyrite
M314	Vernerov (Chequia)	Chalcopyrite, galena, sphalerite, stannite
M395	Herbeumont (Belgium)	Galena, marcasite, pyrite, sphalerite
M67	Kipushi (Congo)	Bornite, chalcopyrite, covellite, galena, sphalerite, tetrahedrite

figure 1 having nicely individualized clusters of pixels in the spectral domain that would correspond to each mineral specie. As can be seen from *figure 3*, the image pixels instead of being strongly clustered occupy a continuum of colours scattered along the black to white bisector of the RGB cube.

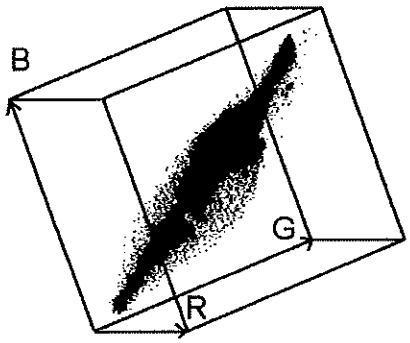

Figure 3. – Plot of pixel signatures in the RGB space for the Kipushi copper ore from figure 2.

Figure 3. – Nuage de points dans l'espace RGB correspondant aux signatures spectrales des pixels de l'image du minerai de Kipushi (fig. 2).

This can be attributed to polishing defects that tarnish the reflectance of a mineral as well as to the mixing of signatures (called mixels in remote sensing) occurring at the interface between two different species.

Four methods for the classification of pixels

Introduction

Classification procedures, more often called segmentation procedures in imaging, form a large group of techniques ranging from the basic thresholding operation to the most sophisticated methods of multivariate clustering. These methods can be broadly subdivided into supervised and unsupervised classifications. In the first series of techniques, a learning step allows the operator to select so-called training sets representative of each individual mineral within the image. The unsupervised classifications are based on automatic identification of clusters in the spectral space and require no operator selection. Unsupervised classifications are left aside in this paper, because a given ore is made out of a restricted number of economic minerals that can be learned to the system in a reasonable time. Supervised is assumed to be superior to unsupervised in such conditions.

The statistics gathered from the user-defined training sets (or the clusters) serve to design various classification criteria. The simplest example of supervised classification in colour imaging is threefold thresholding (also known as the parallelepiped method) whereby all pixels falling within a given box in the RGB space are assigned to the same mineral.

Table II gives the six univariate statistics gathered for chalcopyrite

$$\left\{\left(\mu_{Cp}^{R},\sigma_{Cp}^{R}\right);\left(\mu_{Cp}^{G},\sigma_{Cp}^{G}\right);\left(\mu_{Cp}^{B},\sigma_{Cp}^{B}\right)\right\}$$

TABLE II. – Univariate statistics for the chalcopyrite ($CuFeS_2$) and sphalerite (ZnS) training sets in Panasqueira.

TABLEAU II. – Statistiques univariées pour les plages d'apprentissage de la chalcopyrite ($CuFeS_2$) et de la sphalérite (ZnS) de Panasqueira.

	Red		Green		Blue	
	mean	std dev.	mean	std dev.	mean	std dev.
Sphalerite I (EP833)	83.73	1.9	80.36	1.4	81.58	2.1
Chalcopyrite (EP833)	173.49	1.8	151.1	1.5	110.6	2.2

and it can be said from normal distribution theory that any given pixel $\{r^R, r^G, r^B\}$ corresponds to chalcopyrite if and only if :

$$r^R \in \left[\mu^R_{Cp} \pm 2\sigma^R_{Cp}\right] \text{ and } r^G \in \left[\mu^G_{Cp} \pm 2\sigma^G_{Cp}\right] \text{ and } r^B \in \left[\mu^B_{Cp} \pm 2\sigma^B_{Cp}\right] \quad [1]$$

with :

μ^R_{Cp} : arithmetic mean of the red reflectance values in the chalcopyrite training set,

σ^R_{Cp} : the standard deviation of the red reflectance values in the chalcopyrite training set,

r^R : the intensity (reflectance) of a given pixel in the red image.

Such a technique can be implemented on any image analyzer and would give reasonable results if, and only if, minerals gave widely separated clusters in the RGB space which is contradicted in practice by *figure 3*. Moreover, from the poor occupation of the RGB cube, it is obvious that chrominance information plays a secondary role with respect to intensity. Hence, the classification results obtained by thresholding of colour images is often improved by simply converting RGB images into hue, saturation, intensity images (7). Another approach is to perform principal component analysis and to apply thresholding on the two resulting images.

Although, thresholding is a very simple and intuitive operation, it makes little sense ignoring potential correlation between the colour channels when true multivariate classification techniques are routinely available on modern computers. These multivariate techniques will allow to design more subtle classification criteria using combined information from the red, green and blue channels.

In order to evaluate the relative performance of some multivariate discriminant procedures, we have chosen four different methods that will be briefly synthesized hereafter.

Let us assume m minerals in an image corresponding to populations of pixels designated by $\{M_1, ..., M_m\}$. The corresponding training sets of pixels sampled by the operator are designated by $\{T_1, ..., T_m\}$. Let us indicate the spectral signature of a given pixel by a vector $r = \{r^R, r^G, r^B\}$. The basic idea behind any classification principle will be to assign r to the mineral φ such that the probability that r belongs to M_φ (noted P (M_φ/r) is maximal.

$$P(M_\varphi / r) = p_\varphi f_\varphi(r) \text{ with } \varphi = 1,....,m \quad [2]$$

where p_φ is the a-priori probability (generally equal to 1/m unless specified) and $f_\varphi(r)$ is the posterior probability of mineral φ corresponding to the observed pixel location (r) in the RGB space.

Multigaussian quadratic classification

Multigaussian quadratic discriminant analysis is a very popular tool implemented in most statistical packages (DSCRM routine from IMSL STAT in this study). The basic assumption is that red, green and blue reflectance intensities obey reasonably gaussian distributions. *Figure 4* illustrates that this is acceptable in ore microscopy if a careful image acquisition procedure has been used. If the histograms display a positively skewed trend than the quality of polishing or the image acquisition conditions must be incriminated. In the RGB hyperspace, the 20 × 20 pixels selected as representative training sets for the various mineral specie plot as ellipsoidal clouds (*fig. 5*). The supervised learning procedure gives m training sets whose parameters (mean and covariance matrix) can be estimated by maximum likelihood as :

$$\mu_\varphi = \frac{1}{N}\sum_{j=1}^{N} r_{\varphi j} \quad \text{with } \varphi = 1, ..., m \quad [3]$$

$$\Sigma_\varphi = \frac{1}{N}\sum_{j=1}^{N}(r_{\varphi j} - \mu_\varphi)(r_{\varphi j} - \mu_\varphi)^t$$

where N is the number of pixels in the training sets (typically N = 400 arranged in a 20 × 20 window in the present case).

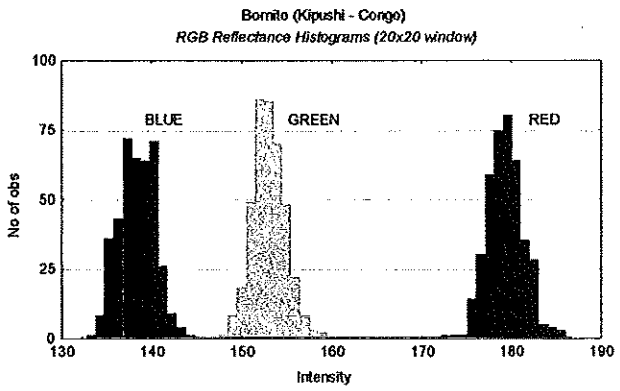

Figure 4. – Red, green and blue reflectance histograms of the brown bornite (Bo/B) training set from figure 2 indicating reasonably normal distributions.

Figure 4. – Histogrammes de réflectance R,G et B des plages d'apprentissage de la bornite brune (Bo/B) (fig. 2) indiquant une distribution raisonnablement normale.

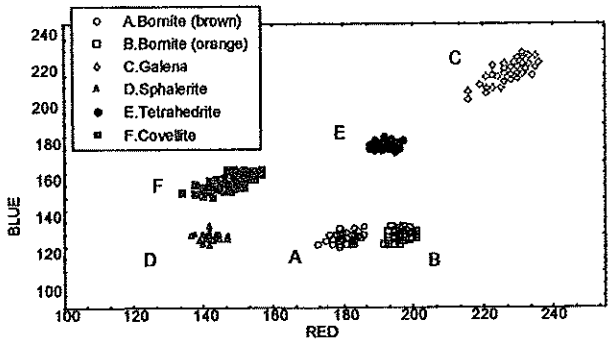

Figure 5. – Scatterplot of the red vs. blue reflectances corresponding to six training sets for minerals present in the Kipushi sulphide paragenesis.

Figure 5. – Nuage de points des réflectances dans le rouge et dans le bleu correspondant aux six plages d'apprentissage des minéraux présents dans la minéralisation sulfurée de Kipushi.

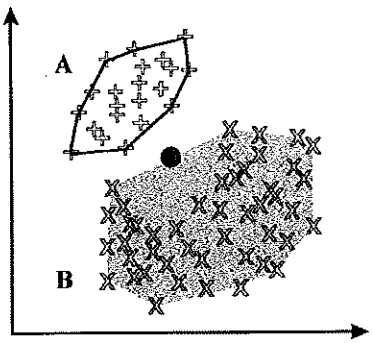

Figure 6. – According to the nearest neighbour rule pixel (●) will be classified as phase A whereas it would be attributed to phase B using the convex hull criterion.

Figure 6. – Selon le critère de classification par le plus proche voisin, le pixel (●) sera classé A tandis qu'il serait classé B en se basant sur le critère d'enveloppe convexe.

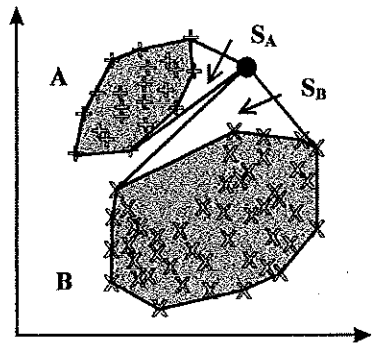

Figure 7. – The convex hull criterion will classify pixel (●) as phase A rather than phase B because the area (volume) of the increment S_A is greater than the increment S_B.

Figure 7. – Le critère de l'enveloppe convexe classera le pixel (●) comme étant de la phase A plutôt que de la phase B car l'incrément d'aire (volume) S_A est supérieur à l'incrément S_B.

The classification procedure proceeds by computing for each pixel vector *r* its probability to belong to mineral φ using the estimator for the gaussian distribution :

$$f_\varphi(r) \propto \exp\left[-(r-\mu_\varphi)^T \Sigma_\varphi^{-1}(r-\mu_\varphi)/2\right] \qquad [4]$$

Nearest neighbour classification

Instead of using a parametric method relying on the assumption of normality for reflectance signatures, it is also possible to use non-parametric method based on the estimation of a posterior probability. A popular method is the k-nearest neighbour classification, assigning a pixel to the most represented mineral φ within the group of nearest neighbours in the spectral hyperspace. The number (k) of nearest neighbours and the distance metric to be used is left to the operator. In the present study we have used the simplest version of this algorithm consisting in searching for each pixel its unique closest neighbour and assigning to it the same mineral phase. The metric used is the euclidean distance (*fig. 6*). A maximum distance criterion can be fixed at an arbitrary value to avoid classifying pixels that are judged too far away from the training set.

Convex hull classification

Considering pixels as realisations of a stationary Poisson process in the spectal hyperspace, it is also possible to estimate a posterior probability $f_\varphi(r)$ using the Lebesgue measure λ(.) of the domain D_φ occupied by mineral φ. The a priori probability p_φ is taken equal to $\lambda(D_\varphi)/l(D)$ where D is the union of all domains (D_1, ..., D_φ). In practice, the Lebesgue measure of each domain D_φ in the RGB space is estimated by the volume of the convex hull $V[H(T_\varphi)]$ of the training set T_φ given by the supervised learning process for component φ. According to the classification rules, any given pixel of signature *r* is assigned to the component for which a minimal expansion of the convex hull volume allows to include *r* (*fig. 7*). Pixels falling within the convex hull of class φ, are automatically classified as φ, whereas pixels belonging to more than one hull are classified according to a recursive algorithm detailed in (8). Possibly, a user-defined maximum expansion can be implemented to avoid classifying pixels that are judged too far away from the training set. *Figure 6* graphically illustrates the main differences between nearest neighbour and convex hull classification.

Behavioural classification

Behavioural classification is based on the hypothesis of a non-stationary Poisson process. In order to estimate the density $f_\varphi(r)$ within a given region of the RGB space, a uniform kernel K(.) estimator is used :

$$f_\varphi(x) = \frac{1}{n_\varphi (2h_\varphi)^3} \sum_{i=1}^{n_\varphi} K\left(\frac{x - x_{\varphi i}}{h_\varphi}\right) \qquad [5]$$

where :

$x_{\varphi i}$ are the n_φ pixels in the training set of mineral φ,

h_φ is the window bandwidth.

Mineral		Segmentation		
		Multigaussian	Convex Hull	Behavioural
EP833/1	/sphalerite	25.29	24.27	21.78
	/arsenopyrite	9.37	9.07	8.86
	/pyrite	4.80	5.36	3.87
	/chalcopyrite	33.26	35.76	31.30
	/pyrrhotite	5.56 (1)	1.10	0.53
M314/1	/chalcopyrite	11.74	11.03	10.13
	/stannite	41.28	42.31	38.48
	/sphalerite	30.23	32.58	31.36
	/galena	3.16	2.84	2.56
M395/2	/sphalerite	7.84	10.84	5.75
	/galena	31.44	30.31	23.78
	/pyrite	19.52	9.17	10.37
	/marcasite	8.07	18.70	14.49
M67/2	/galena	13.79	13.39	12.94
	/sphalerite	39.08	39.10	37.53
	/bornite brown	7.60	7.49	6.52
	/bornite orange	15.12	15.27	15.06
	/tetrahedrite	17.14	18.59	15.55

TABLE III. – Comparison between phase ratios obtained in four images using three different segmentation techniques. Gangue minerals and unclassified pixels are not indicated. Behavioural classification is systematically too pessimistic. Convex hull is less sensitive to mixels than multigaussian and probably gives the best estimate of phase ratios. (1) : Erroneous pyrrhotite pixels were detected in the optical transitions between pyrite and chalcopyrite.

TABLEAU III. – Comparaison entre les pourcentages de phases obtenus sur quatre images en utilisant trois méthodes de segmentation différentes. La fraction de gangue ou de pixels non-classés n'est pas indiquée. Les estimations par la méthode « behavioural » sont systématiquement trop pessimistes. La méthode de l'enveloppe convexe est moins sensible aux mixels que la multigaussienne et fournit probablement les meilleurs estimations. (1) : correspond à de la pyrrhotine virtuelle identifiée dans les zones de transition pyrite/chalcopyrite.

In practice, the window bandwidth is not chosen as constant, but depends on the variance of the training sets. The average third nearest neighbour distance within each mineral's training set is often used as h_φ.

Because training sets are never randomly sampled, an additional optimization of the prior probabilities is also required (8). Finally, the classification procedure assigns a pixel to the mineral φ for which the added intensity is minimal. With respect to the convex hull classification, the rule is thus based on the intensities within convex hulls rather than simply on the volumes of these hulls.

■ COMPARATIVE SEGMENTATION OF COLOUR MINERALOGRAPHIES

The five mineralographies used in this study were submitted to an expert for correct identification of the training sets. This step was of primary importance in order to avoid including scratches and pits in the training sets and thereby artificially widening their variance. Afterwards, several variants of the segmentation procedures described in the previous paragraphs were tentatively tried on the images.

It is obviously impossible to present the complete set of images after segmentation, so that we have chosen to restrict ourselves to the most striking differences. Apart from visual comparison, it is also very difficult to establish a quantitative performance criterion. The correct procedure would be to proceed to a manual classification of a random subset of pixels and to compare it with the segmentation results (9). This is known as ground truth analysis in remote sensing but can hardly be achieved under the microscope due to limited resolution. Instead, we have chosen to compute surface ratios as indicators of the precision to be expected from these measurements. But, this should not be considered as a measure of performance of the segmentation procedure (*table III*).

Visual evaluation of segmentation procedures

As a general observation the following comments apply to the four methods presented in this paper.

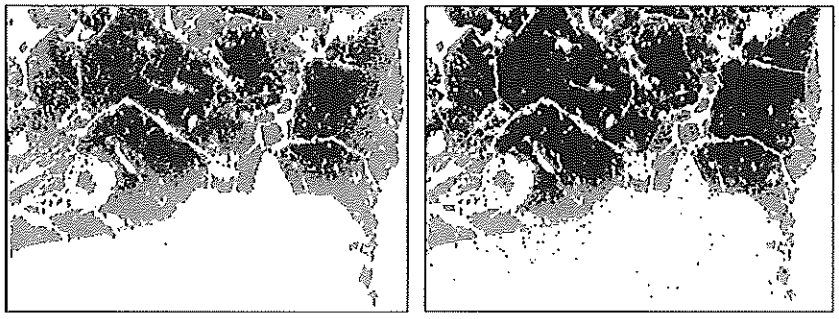

Figure 8. – Multigaussian (left) and nearest neighbour (right) classifications of pyrite (grey) and marcasite (black) in image of Herbeumont. Due to substantial overlapping of the training sets, all non parametric classifications clearly outperform the multigaussian procedure (table III).

Figure 8. – Classifications multigaussienne (gauche) et selon le plus proche voisin (droite) de la pyrite (gris) et de la marcassite (noir) de Herbeumont. En raison d'un chevauchement significatif des plages d'apprentissage, toutes les méthodes non-paramétriques sont nettement supérieures à la méthode multigaussienne (tabl. III).

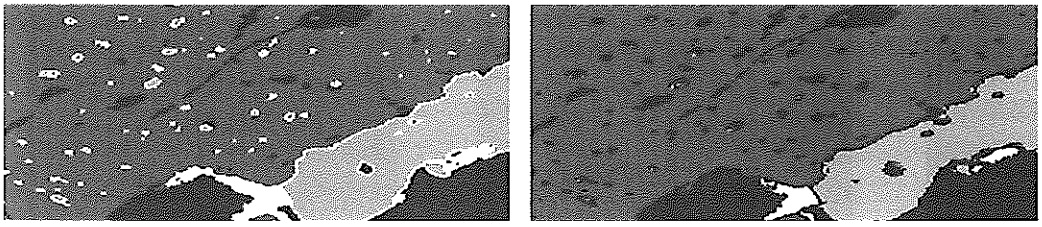

Figure 9. – Convex hull (left) and behavioural (right) classifications on a sphalerite disease pattern in M314/1. Convex hull catches the small chalcopyrite (light grey) inclusions in sphalerite (dark grey). The thin stannite (white) rims between chalcopyrite and sphalerite are due to a « mixel effect ». Reflectance values for stannite are perfectly intermediate between chalcopyrite and sphalerite. Black pixels are gangue. The behavioural classification leaves a lot of pixels (and mixels) unclassified (black). Aspect ratios of the images have been modified (2:1).

Figure 9. – Classifications par l'enveloppe convexe (gauche) et par la méthode « behavioural » (droite) dans la section M314/1. La méthode par l'enveloppe convexe capte bien les petites inclusions de chalcopyrite (gris clair) dans la sphalérite (gris foncé). La fine bordure de stannine (blanc) entre chalcopyrite et sphalérite est due à des « mixels ». Les valeurs de réflectance de la stannine sont exactement intermédiaires entre chalcopyrite et sphalérite. Les pixels noirs correspondent à de la gangue. La méthode « behavioural » laisse beaucoup de non-classés (noir). Les images ont été déformées selon un rapport (2:1).

Multigaussian

Multigaussian classification is well suited for reflected light microscopy, because ideal image acquisition should lead to normal reflectance distributions. However, due to the estimation of mean and variance parameters, this method is particularly sensitive to a bad selection of the training sets (departure from the normality assumption) and the occurrence of abundant scratches, fractures or microhardness fringes in the section will strongly affect the overall segmentation.

It is the operator's responsibility not to forget a possible mineral specie in the training procedure if no constraints are used in terms of confidence interval.

The multigaussian segmentation is much less efficient in case different minerals display overlapping training sets (*fig. 8*).

Single nearest neighbour

Due to its non parametric nature, nearest neighbour segmentation is quite robust to a bad selection of the training sets or to the degradation of the image. Transition zones between different minerals are sharper than in multigaussian classification. However, in case of strongly overlapping training sets, this method performs less well than the convex hull classification.

Convex hull

Convex hull classification is robust with respect to a modification of the training sets. It always gives superior results with respect to multigaussian, although spectral signatures of minerals do not obey a stationary Poisson point process. Overall performance is similar to single nearest neighbour classification but less noisy. The convex hull method displays a good resistance to an increasing amount of mixels (*fig. 9 and 10*)

Behavioural

For the set of images tested in this paper, the behavioural classification is very similar to the convex hull classification. The automatic fitting of the window bandwidth as a function of the variance as used here was often too pessimistic and, as a consequence, a large amount of pixels were still left unclassified. Surprisingly, the segmentation gives superior results if more heterogeneous surfaces are selected in the training sets. Instead of searching for perfectly polished zones, it seems better to sample surfaces of intermediate quality.

Geometric analysis of segmented images

The ability of a segmentation procedure to correctly classify pixels corresponding to a given mineral not only depends on the spectral signature, but mostly on the other conflicting phases that are present and on the spatial connexity between these phases. As an example of this, stannite in the presence of chalcopyrite and sphalerite is very easily identified, but the phase ratio of stannite can be overestimated if

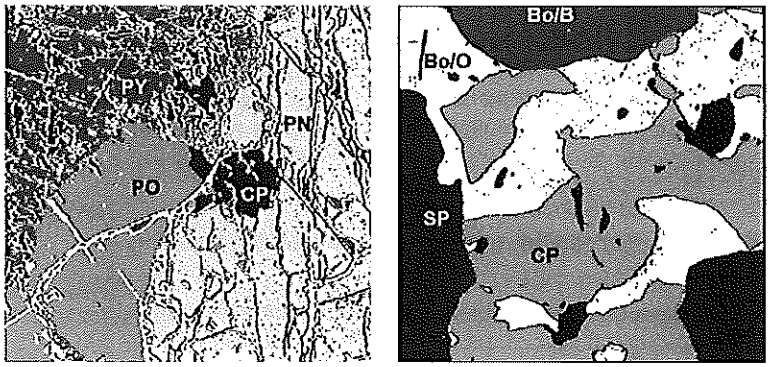

Figure 10. – Result of convex hull classification on images from Sudbury (M12) and Kipushi (M67) mineralizations. Misclassification is minimal but still occurs between very similar mineral species (e.g. pyrite(PY) and pentlandite (PN)) or in transition zones (e.g. virtual brown bornite (Bo/B) is detected between orange bornite (Bo/O) and chalcopyrite (CP)).

Figure 10. – Illustration de la classification par enveloppe convexe sur les images de Sudbury et de Kipushi. Le déclassement est minimal mais est toujours perceptible entre des phases minérales très proches (exemple la pyrite (PY) et la pentlandite (PN)) ou dans les zones de transition (exemple : de la bornite brune virtuelle (Bo/B) est identifiée entre la bornite orange (Bo/O) et la chalcopyrite (CP)).

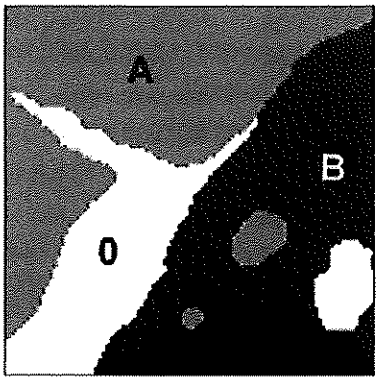

Figure 11a. – Composite image with pixels assigned to phase A or B and spectrally undetermined regions (0).

Figure 11a. – Image composite de pixels attribués aux phases A ou B et de régions spectralement indéterminées (0).

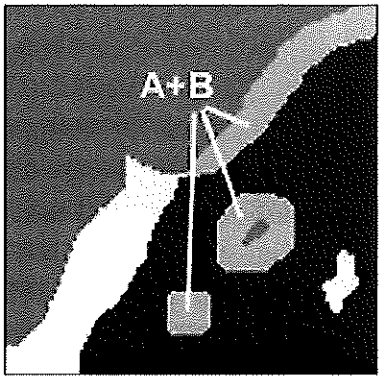

Figure 11b. – After summing up the individual dilations performed on A and B new undetermined regions (A + B) are created.

Figure 11b. – Par addition des images de A et de B dilatées individuellement, de nouvelles régions indéterminées (A + B) sont créées.

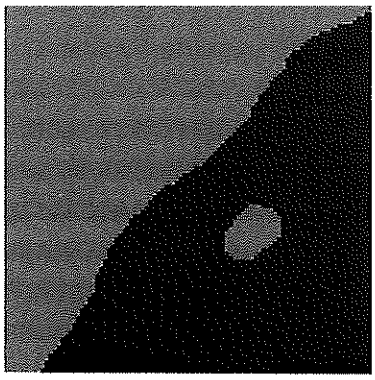

Figure 11c. – The geodesic propagation of A and B solves the spectral indetermination by using a proximity criterion.

Figure 11c. – La propagation géodésique de A et de B résout l'indétermination spectrale en ayant recours à un critère de proximité spatiale.

the connexity between chalcopyrite and sphalerite is important. The increment of « virtual stannite » (most often mixels of chalcopyrite and sphalerite) generated this way might be as important as 2-3 % of the total image area which added to minor ore minerals generates a large relative estimation error. Although by no way a manner of judging the quality of segmentations, the measure of phase ratios in different segmented images tells us about the variability of this measure. *Table III* presents some typical results obtained for multigaussian, convex hull and behavioural classifications.

■ CONTEXTUAL FILTERING

A closer look at the phase-labelled images obtained after segmentation reveals a complex spatial relationship between classified and unclassified pixels (*fig. 8 to 10*). Typically, unclassified pixels will appear as holes or fractures within a grain whereas classified pixels of say phase A may appear as speckles within a homogeneous zone classified as being phase B. Instead of considering such speckles as being inclusions or exsolutions, it is often more realistic to consider them as spectral noise and add these pixels to the list of unclassified pixels.

In practice, this can be realized by performing the following operations :

- take each one of the φ binary images obtained after segmentation and perform a binary dilation of desired width λ (e.g. $\lambda = 2$) ;
- multiply the image of the φ^{th} mineral phase by a factor of $2^{\varphi}(1,2,4,8,16,...)$;
- add the set of φ images obtained after multiplication.

By doing this, one ends up with a composite image wherein clearly classified pixels are at values of 2^{φ}, whereas ambiguously classified pixels are at any non 2^{φ} value (e.g. a value $21 = 16 + 4 + 1 = 2^4 + 2^1 + 2^0$ is due to a pixel being classified after dilation as either phase 4, 2 or 0).

The consequence of a dilation of size λ is such that all pixels lying within a distance of less than λ pixels to a phase A/phase B transition are labelled as A + B (*fig. 11b*).

Considering that the final result of a segmentation has to be an image where no pixel is left unclassified, a geodesic propagation (10, 11) is performed to classify the spectrally undetermined domains. The practical result of this is that all unclassified pixels are assigned a value corresponding to the code of the nearest classified pixel (*fig. 11c*). Thanks to the previous dilation process, the geodesic propagation step fills in undetermined A + B zones and acts as a filter removing noisy pixels within well classified domains. This kind of filtering is considered as a contextual filter, because it selectively removes isolated pixels lying within well classified regions without affecting isolated pixels scattered in an undetermined region of the image (*fig. 12*). *Figure 13* displays the final result obtained after convex hull segmentation and contextual filtering (with a dilation of size $\lambda = 2$) on a mineralography from the Sudbury mineralization. *Table IV* indicates the influence of contextual filtering on the phase

TABLE IV. – Comparison between phase ratios obtained before and after contextual filtering of a convex hull segmentation in the Sudbury mineralization.

TABLEAU IV. – Comparaison entre les pourcentages de phase obtenus avant et après filtrage contextuel dans la minéralisation de Sudbury.

		Before filtering	After filtering
M12/1	/pyrrhotite	27.73	27.71
	/pentlandite	33.62	35.86
	/pyrite	17.68	24.13
	/chalcopyrite	7.68	9.89
	/gangue	0.6	1.77

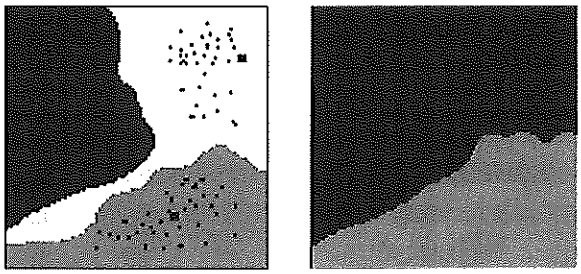

Figure 12. – Contextual filtering dissolves the isolated black pixels lying within the grey phase whereas it uses the others to fill in the white undetermined region.

Figure 12. – Le filtrage contextuel permet de dissoudre les pixels noirs disséminés dans la phase grise tandis qu'il utilise les autres pour inonder la région indéterminée (blanc).

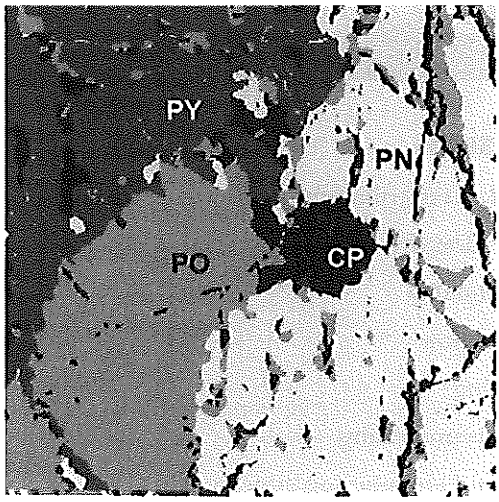

Figure 13. – Convex hull segmentation (fig. 10) followed by contextual filtering $\lambda = 2$ in Sudbury mineralization (M12/1).

Figure 13. – Segmentation par enveloppe convexe (fig. 10) suivie d'un filtrage contextuel $\lambda = 2$ dans la minéralization de Sudbury (M12/1).

ratio of the different minerals. It is noticeable that a significant amount of pyrite pixels were first misclassified as pentlandite by the convex hull segmentation, but contextual filtering improved this segmentation by densifying the pyrite regions and eliminating noisy pixels.

■ CONCLUSION

Although it will probably never become an infallible *push button* technique, colour image analysis appears to be a valuable alternative to electron microscopy and EDX mapping if careful image acquisition techniques are used. This paper contributes to the definition of a systematic procedure for correct digitization of images in ore microscopy. It demonstrates how even the simplest segmentation techniques can give reasonable results in phase ratio estimations of minerals with very similar spectral signatures like pyrite, marcasite and pentlandite for example. It is obvious that bireflectance and pleochroism will strongly affect the performance of any segmentation procedure if nothing is done to take this variability into account. Further work with polarized light microscopy will be dedicated to this problem of dealing with anisotropic minerals and a larger number of other minerals, particularly iron oxydes, will be investigated to determine the limits of mineral identification using colour image analysis. The automatic identification of opaque minerals under the optical microscope is probably not a reasonable objective, but correlation between intensities in digital images and reflectance spectra as published in the IMA-COM QDF (5) are being investigated.

Acknowledgements

This work largely benefited from the meticulous investigations of Simone Tarquini (Pisa) during his stay in Liège and in Madrid with our friend Ricardo Castroviejo. We would like to thank Alan Criddle for his help with reflectance standards and Jean-François Nivart and Yves Daoust (Euresys S.A.) for the fruitful discussions we had on colour imaging and video signals.

references

(1) PETRUK (W.). – The MP-SEM-IPS image analysis system, in « Short course on image analysis applied to mineral and earth sciences », ed. W. Petruk, Mineralogical Association of Canada, 16 (1989).

(2) SUTHERLAND (D.), GOTTLIEB (P.). – Application of automated quantitative mineralogy in mineral processing. **Minerals Engineering**, 4 (1991), p. 753-762.

(3) PILLER (H.). – Colour measurements in ore microscopy. **Mineral. Deposita**, 1 (1966), p. 175-192.

(4) GALOPIN (R.), HENRY (N.). – Microscopic study of opaque minerals, Heffer & Sons, Cambridge (1972).

(5) CRIDDLE (A.), STANLEY (C.). – Quantitative data file for ore minerals : 3rd ed., Chapman & Hall, London (1993).

(6) PIRARD (E.), LEBRUN (V.), NIVART (J.-F.). – Optimal acquisition of video images in reflected light microscopy. **European Microscopy and Analysis**, n° 60 (July 1999), p. 9-11.

(7) TRÉMEAU (A.), LOZANO (V.), LAGET (B.). – How to optimize the use of the LHC color space in color image analysis processes. **Acta Stereologica**, 14-2 (1995), p. 223-228.

(8) RASSON (J.P.), GRANVILLE (V.). – Geometrical tools in classification. **Comput. Statistics and Data Analysis**, 23 (1996), p. 105-123.

(9) DE KEERSMAEKER (M.-L.). – Stratégie d'échantillonnage des données de terrain intégrées dans l'analyse des images satellitaires. **L'espace géographique**, 3 (1987), p. 195-205.

(10) LANTUEJOUL (Ch.), BEUCHER (S.). – On the use of the geodesic metric in image analysis. **J. Microsc.**, 121 (1981), p. 39-49.

(11) COSTER (M.), CHERMANT (J.-L.). – Précis d'analyse d'images, Ed. du CNRS, Paris (1989).

"Gratitude is something of which none of us can give too much. For on the smiles, the thanks we give, our little gestures of appreciation, our neighbors build up their philosophy of life."

A. J. Cronin, Scottish novelist

Merton C. Flemings Symposium

June 28–30, 2000

Massachusetts Institute of Technology (MIT) Campus, Cambridge, Massachusetts

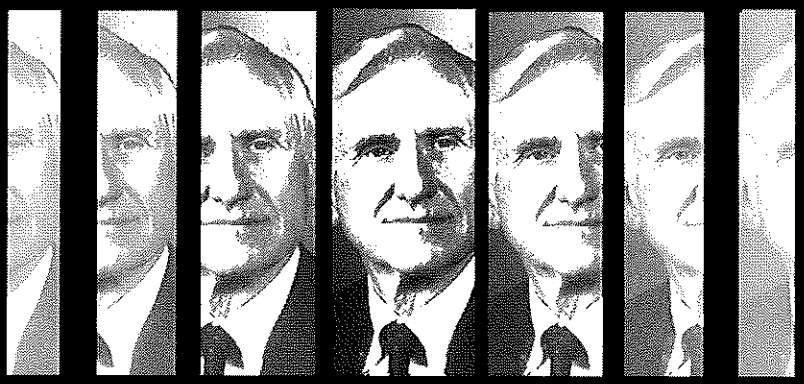

Sponsored by The Minerals, Metals & Materials Society (TMS) and the Department of Materials Science and Engineering of the Massachusetts Institute of Technology (MIT)

In gratitude and appreciation of Merton C. Flemings, TMS and MIT cordially invite you to attend the Merton C. Flemings Symposium.

As an educator, researcher, technology policy leader, mentor, and friend, Merton C. Flemings has made significant contributions to MIT and the materials science and engineering community. In celebration of his accomplishments, the following technical sessions and social events have been scheduled:

Reserve these dates and join Professor Flemings in historic Cambridge, Massachusetts, in June 2000 to celebrate this milestone in his career.

For general and attendance information, please contact the TMS Meeting Services at telephone (724) 776-9000, ext. 243; fax (724) 776-3770; or email mtgserv@tms.org.

TMS
Minerals • Metals • Materials

Technical Sessions

Topics aligned to key contributions by Professor Flemings

Dendritic solidification dynamics

Control of casting quality

Interdendritic fluid flow

Semi-solid processing

Innovative materials processing

Materials science and engineering education

Social Highlights

Reception for arriving guests in The Royal Sonesta Hotel, Boston, MA, on the evening of June 27, 2000
(The Royal Sonesta Hotel will be the headquarters hotel for the symposium)

Banquet at the Museum of Fine Arts in Boston's Back Bay on the evening of June 29, 2000
During the banquet you can enjoy the museum's fine Asian art collection and listen to Yo-Yo Ma, an internationally celebrated cellist.

Furthermore

A distinguished list of speakers has been invited, and all invited and contributed papers will be published in a proceedings volume, along with a selection of Merton C. Flemings's most important papers.

A copy of the proceedings is included as part of the registration fee.

Up-to-date information on this and all TMS-sponsored and cosponsored meetings is available via the World Wide Web at http://www.tms.org/Meetings/Meetings.html